Journal of Solid State Electrochemistry
https://doi.org/10.1007/s10008-020-04853-2

ORIGINAL PAPER

Electrochemical stability of steel, Ti, and Cu current collectors in water-in-salt electrolyte for green batteries and supercapacitors

Walter Giurlani[1] · Luca Sergi[1] · Eugenio Crestini[1] · Nicola Calisi[1] · Federico Poli[2] · Francesca Soavi[2] · Massimo Innocenti[1]

Received: 8 September 2020 / Revised: 21 October 2020 / Accepted: 24 October 2020

Abstract

The electrochemical behaviour of steel, copper, and titanium current collectors was studied in aqueous solutions of lithium bis(trifluoromethanesulfonyl)imide (LiTFSI) at various concentrations, from 0.5 up to 20 m. As the concentration of the electrolyte increases, the electrochemical window of water stability widens according to the "water-in-salt" concept. The metal grids have been studied electrochemically, both under anodic and cathodic conditions, by means of cyclic voltammetry and chronoamperometry. Subsequently, a microscopic analysis with SEM and compositional analysis with XPS was carried out to evaluate the surface modifications following electrochemical stress. We found that copper is not very suitable for this kind of application, while titanium and steel showed interesting behaviour and large electrochemical window.

Keywords Water-in-salt · Current collector · Electrochemical stability · Battery · Supercapacitor

Introduction

Lithium-ion batteries (LIB) are nowadays one of the most important energy storage devices and are currently dominating the consumer electronic market. They have been indicated as the most promising option for the next generation of hybrid and electric vehicles but their possible application for this purpose is still uncertain today mainly because of concerns raised over their safety, cost, and environmental impact [1]. The electrolytes presently used in commercial LIBs are based on mixtures of organic solvents and contain lithium hexafluorophosphate ($LiPF_6$) as lithium salts [2]. The use of these electrolytes allows high performance in terms of energy and cycle life. However, since these electrolytes are flammable and volatile, their use poses serious safety risks and strongly reduces the temperature range of use. Furthermore, it has also been observed that they are particularly aggressive in terms of corrosion towards the working electrodes, under certain operating conditions, consequently reducing the cell performance. Therefore, substantial costs of these systems are incurred not only directly by these electrolytic components but also to a greater extent by the safety management required for the dangerous combination of flammable electrolytes and energy-intensive electrodes that are long-lasting and resistant to corrosion [3, 4]. The main reason for using classical organic electrolytes (acetonitrile or carbonates) was that it permits to design devices with a cell voltage of 2.7–2.8 V.

These organic electrolytes display favourable properties on the negative electrode side, including the formation of a lithium conducting passivation layer on the surface of the electrode, the so-called solid electrolyte interphase (SEI). The presence of this layer extends the electrochemical stability window of the electrolyte at the negative electrode, even with very reducing anode materials, such as metallic Li and lithiated graphite. However, on the positive electrode side, the stability window of these systems limits the number of

In memory of Prof. Roberto Marassi, a great scientist and innovator in electrochemistry for energetics and beyond

Supplementary Information The online version contains supplementary material available at https://doi.org/10.1007/s10008-020-04853-2.

✉ Walter Giurlani
wlater.giurlani@unifi.it

✉ Francesca Soavi
francesca.soavi@unibo.it

[1] Department of Chemistry "Ugo Schiff", Università degli Studi di Firenze, via della Lastruccia 3, 50019 Sesto Fiorentino, FI, Italy

[2] Dipartimento di Chimica "Giacomo Ciamician", Alma Mater Studiorum Università di Bologna, Via Selmi 2, 40126 Bologna, Italy

Published online: 09 November 2020

applicable active materials, especially due to the limited stability of most of these compounds at potentials exceeding 5 V [5].

As a possible solution to these problems, researchers have proposed in recent years the use of aqueous electrolytes inside the cells of lithium batteries. However, pure water as a solvent shows a window of thermodynamic stability too narrow of only 1.23 V, as defined by the decomposition reaction of water [6], which imposes a restriction on the choice of electrochemical couples and consequently the practical energy output of aqueous battery chemistries and cell voltage [7].

On the other hand, the aqueous solutions display important advantages, e.g. higher conductivity, non-flammability of the electrolyte, and low cost, both regarding the electrolyte itself and the separator material. The higher ion conductivity increases the high-power capability of electrochemical cells based on aqueous electrolyte, recently demonstrated with $LiCoO_2$ by Cui et al. and with $LiMn_2O_4$ and hybrid systems by Wu et al. [8, 9].

In general, the aim of the studies in recent years has been to be able to design a system with aqueous electrolytic solutions that have the same performance as cells with organic solvents, and therefore a comparable electrochemical stability window, but which are above all safer, longer lasting, and with less environmental impact.

Recently, relatively large stability windows of up to 3 V have been reported for highly concentrated, "water-in-salt", aqueous solutions of lithium bis(trifluoromethylsulfonyl)imide (LiTFSI) providing an opportunity for the development of high-voltage aqueous batteries [10, 11].

LiTFSI (lithium bis(trifluoromethylsulfonyl)imide) was chosen as the salt because of its high solubility in water (> 20 m at 25 °C) and high stability against hydrolysis. The "water-in-salt" definition applies when the LiTFSI concentration is above 5 m, since the salt exceeds the solvent by weight and volume. In this binary system, the average number of water molecules available to solvate each ion is much lower than the "solvation numbers" which are well established in conventional electrolytes (~ 1.0 m) [12, 13]. The solvation shell is completely different from classical aqueous electrolytes: Li^+ ions are not only surrounded by water molecules but rather by $TFSI^-$ anions together with a limited number of water molecules, depending on the salt concentration. Interionic attractions become more pronounced than solvent-ion interactions causing unusual physicochemical properties. Particularly important is the interphase chemistry on the electrode surfaces which could be modified as a direct consequence of the different cation solvation shell structure. The overall stability window expands as the LiTFSI concentration increases, with both oxygen and hydrogen evolution potentials pushed well beyond the thermodynamic stability limits of water, suppressing water splitting in an extended potential window of 3 V [14].

The first lab-scale batteries utilizing highly concentrated LiTFSI salt in water as the electrolyte were fabricated with stainless-steel current collectors. However, aluminium (Al) is the preferred current collector material on the cathode side of non-aqueous lithium-ion batteries due to its much lower density, higher electronic conductivity, low cost, and the ability to be processed into thin foils by rolling [15–19].

The Pourbaix diagram of Al indicates thermodynamic stability, i.e. the range where passivation due to the air-formed aluminium oxide layer is avoided, only in a small pH range [20]. This small stability window has prevented the use of Al as the current collector in traditional aqueous batteries [21].

In this work, the limits of electrochemical stability of LiTFSI solutions at increasing concentration were evaluated with different metals (steel, copper, and titanium) in order to evaluate their possible use as an anode or as a cathode current collector in aqueous lithium-ion cell. The tests consisted in cyclic voltammetry (CV) and potential step (chronoamperometry) experiments complemented with scanning electron microscopy (SEM) and X-ray photoelectron spectroscopy (XPS) analyses. CVs provided the potential used to define the experimental conditions of chronoamperometry that was used to accelerate current collector ageing and side reactions involving the electrolyte. The corrosion resistance of the metal samples was monitored by observing the trend of the recorded current, at a given potential, as a function of time, and the evolution of the metal surfaces after the ageing tests. The study demonstrates that, despite the recognized wide electrochemical stability of superconcentrated LiTFSI solutions, for practical applications it is important to evaluate the right combination between current collector and salt concentration.

Experimental

Materials

Three commercial meshes made of different metals were chosen as samples: steel (3SS5-050 ANF, Dexmet), titanium (5Ti-7-077, Dexmet), and copper (Grid-CTD-Cu-140mm, Lamart). Meshes of different materials had different thickness and holes; the effective contact area of each sample is reported in Table 1.

Lithium bis(trifluoromethanesulfonyl)imide (LiTFSI) salt, used as electrolyte, was purchased from Sigma-Aldrich and

Table 1 Effective contact area per 1 cm^2 of sample

Sample	Contact area (cm^2)
Copper	0.715
Steel	1399
Titanium	1369

used without further purifications. Solutions of 0.5, 5, 10, and 20 m (mol/kg) of LiTFSI in Milli-Q water were used.

All electrochemical tests were carried out in a glass cell with a three-electrode configuration (Fig. S1). Before each electrochemical measurement, the solution was deaerated with nitrogen for 30 min directly in the cell. Then, the bubbling was interrupted maintaining a nitrogen flow over the solution. Metal meshes with a 1×1 cm^2 section were used as working electrode (WE). Before each analysis, the samples were washed with acetone in ultrasonic bath, rinsed in ethanol, and left to dry.

Carbon paper (2050A-1050, Spectracarb) was used as counter electrode (CE). To increase the active area of the CE, a suspension of activated carbon was drop-casted on the carbon paper following this procedure: (i) 10 mg/mL of activated carbon (CV-XC72R, Fuel Cell Earth) was dispersed in 1-methyl-2-pyrrolidinone (Sigma-Aldrich), containing 1 mg/mL polyvinylidene difluoride (PVDF, Sigma-Aldrich) as a binder to keep the powder bound to the substrate; (ii) 0.5 mL of suspension, equivalent to 5 mg of activated carbon, was drop-casted on the carbon paper; (iii) the solvent was evaporated at 130 °C by placing the electrode on a heating plate; (iv) during the measurements, the counter electrode was wrapped in a glass microfiber filter (Whatman grade GF/A) to prevent any detachment. The high surface area capacitive counter electrode can balance the charge stored by the working electrode during the polarization of the latter and this avoids undesired side reaction at the counter electrode.

Silver wire was used as pseudo-reference electrode (RE), and all potentials were converted to the Li/Li^+ electrode scale. In text, we referred to positive and negative potential with respect to the equilibrium potential represented from the open-circuit potential, recorded before each electrochemical measurement.

The electrochemical tests were performed by a multichannel potentiostat (Metrohm μ-autolab, model Fra-2 Type 3). Cyclic voltammetric scans (CV) were carried out in order to evaluate the anodic and cathodic stability limits of the different metals in LiTFSI aqueous solutions at increased salt concentration and at a scan rate of 20 mV/s. Before CV, the relative OCP (open-circuit potential) value was calculated for each metal, which is characteristic of each material. Then, two measurements were then carried out towards only negative potentials or only positive potentials with respect to the previously recorded OCP value. The potential of the voltammetric cycles was increased until very intense anode or cathode currents were observed. The voltammetric anodic and cathodic limits were used to define the experimental conditions of chronoamperometry that consisted in applying different potentials over 30 min. The current density was calculated considering the effective area of the metals (Table 1).

Microscopic and spectroscopic characterization

Scanning electron microscopy (SEM) analyses were performed with a Hitachi S-2300 equipped with a Thermo Scientific Noran System 7 detector and analysed with Pathfinder software.

X-ray photoelectron spectroscopy (XPS) was used to evaluate the superficial composition of the samples before and after the chronoamperometric stress. The instrument is equipped with a non-monochromatic X-ray source (VSW Scientific Instrument Limited model TA10, Al Kα radiation, 1487.7 eV) set to work at 120 W (12 kV and 10 mA) and a hemispherical analyser (VSW Scientific Instrument Limited model HA100, Manchester, UK). The analyser was equipped with a 16-channel detector and a dedicated differential pumping system maintaining the pressure in the chamber to the 10^{-8} mbar range. The pass energy was set to 22 eV. The measured spectra were analysed using CasaXPS software (version 2.3.19, Casa Software Ltd., Teignmouth, UK). The inelastic background was subtracted using Shirley's method [22], and mixed Gaussian and Lorentzian contributions were used for each component. Calibration of the spectra was obtained by shifting to 284.8 eV, the lowest component relative to the 1s transition of carbon for adventitious carbon [23].

Before SEM and XPS measurements, the metals were rinsed with water and dried.

Results and discussion

Electrochemical measurements

Steel

Figure 1a reports the linear sweep voltammetries carried out at 20 mV/s with steel in LiTFSI solutions at different salt concentrations. Increasing the electrolyte concentration from 0.5 up to 20 m the stability increases in both the anodic and in the cathodic branch of the voltammogram. The anodic onset does not differ much between the three solutions with lower concentration (≈ 4.25 V) but it increases by 10 mV in the case of the 20 m solution. On the other hand, the cathodic onset shows a greater shift with the increase of the electrolyte concentration, reaching 1.84 V for 20 m solution, for an overall window of 2.50 V.

Figure 1b reports the CV run in the lowest potential range after the first linear sweep experiments. The presence of anodic and cathodic peaks suggests that during the first cathodic scan, redox couples are formed on the metal surface as the result of the decomposition of the salt. Increasing the salt concentration, the peak current decreases significantly as well as the potential related to H_2 evolution shifts to more negative values. This is in agreement with the parallel decrease of H_2O concentration.

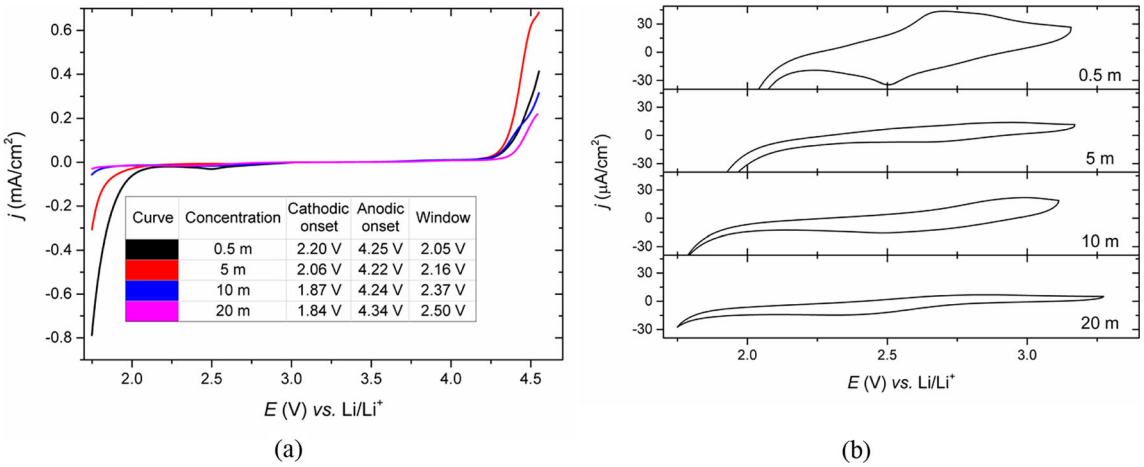

(a) (b)

Fig. 1 (a) Linear sweep voltammetries and (b) CVs in the lowest potential range of steel in aqueous LiTFSI solutions at different salt concentrations

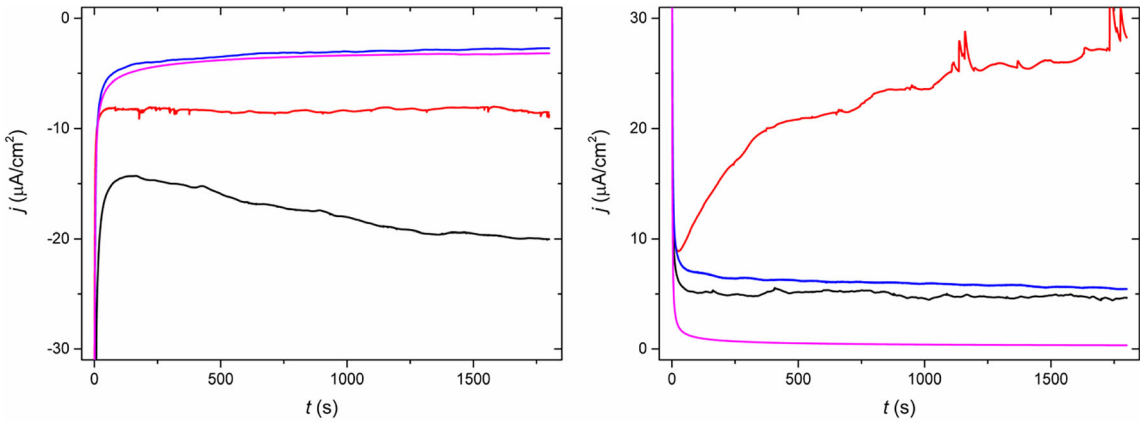

(a) (b)

Fig. 2 Chronoamperometric measurements performed at constant potential of (a) 2.25 V (cathodic) and (b) 4.25 V (anodic). Black, 0.5 m; red, 5 m; blue, 10 m; pink, 20 m

We investigate the evolution of the degradation process occurring on the surface of steel by keeping the electrode at different potentials over 30 min and recording the current. The same potential was used for each solution to compare the different behaviours. The cathodic ageing was carried out at 2.25 V, while the anodic one was performed at 4.25 V. The cathodic tests (Fig. 2a) showed that the current decreased and was

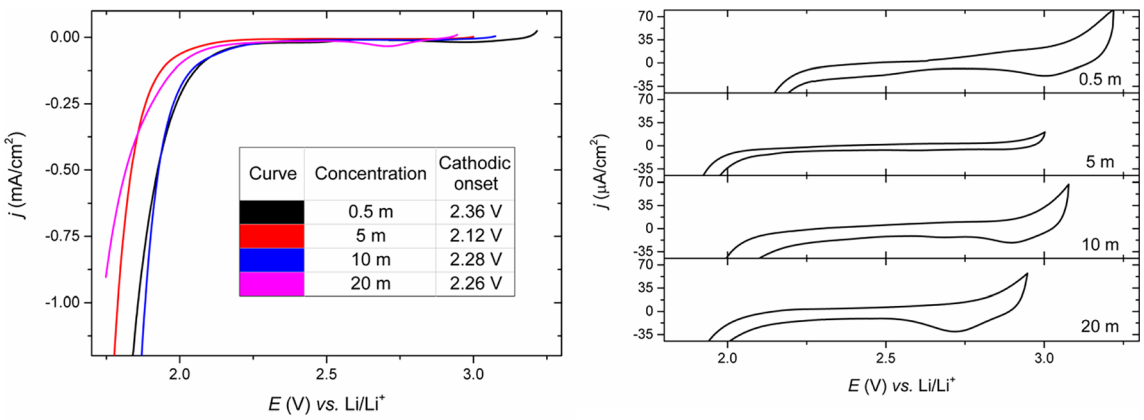

(a) (b)

Fig. 3 (a) Linear sweep voltammetries and (b) CVs in the lowest potential range of copper in aqueous LiTFSI solutions at different salt concentrations

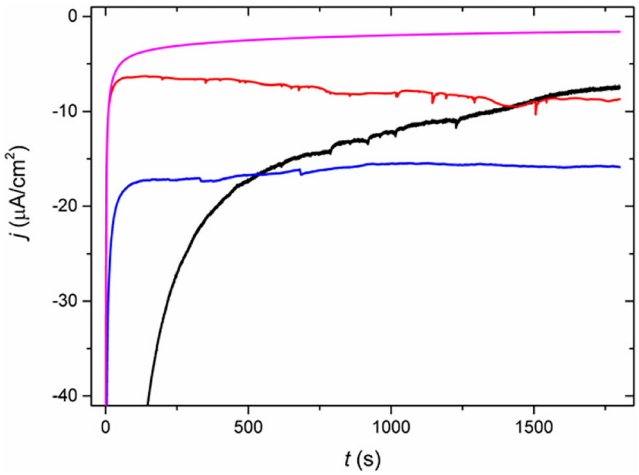

Fig. 4 Chronoamperometric measurements performed at constant potential of 2.25 V (cathodic). Black, 0.5 m; red, 5 m; blue, 10 m; pink, 20 m

more stable for the electrolytic solutions with the highest concentration. The curves recorded with 10 m and 20 m solutions almost overlapped. As it concerns the anodic test (Fig. 2b), the lowest current that was negligible after 30 min was obtained by far using the solution with 20 m concentration. During the anodic stresses, the trend did not completely follow that of concentrations. In fact, unexpectedly, in the 5 m solution, the current did not reach a stationary value but increased during the tests, therefore suggesting that the steel was going against corrosion much more quickly than in the 0.5 m solution.

Copper

Unlike the other metals, copper undergoes through strong corrosion for every concentration of the salt if the applied potential is more positive than the OCP. For this reason, we recorded the behaviour of copper only in the cathodic potential range. The onset of the reduction of hydrogen started at potentials more positive than those observed in the case of steel. Moreover, the onset potentials trend did not follow that of the salt concentration (Fig. 3a). Indeed, in the 0.5 m and 10 m solutions, copper featured a similar behaviour with an anodic limit more positive than that achieved with the 5 m and 20 m solutions. The CV (Fig. 3b) currents are higher with copper than with steel even for high salt concentration. This indicates that the decomposition of the electrolyte is more pronounced in the case of copper with respect to steel. Also, the presence of CV peaks indicates that the passivation layer eventually formed on the metal is not stable. Indeed, a stable passivating layer would insulate the electrode from the solution and, therefore, give rise to very low voltammetric currents.

The chronoamperometric measurement (Fig. 4) was carried out applying a fixed potential of 2.25 V. Also, in this case, as for the onset potentials, there is no direct correlation between the chronoamperometric behaviour and the concentration of the solution. Despite this, solutions with a lower concentration seem to be slower to reach a constant current, suggesting the presence of corrosion reactions at the interphase. The 10 m solution reaches a steady current quickly but maintaining a considerably high value. Only in the case of the 20 m solution does it appear that a stable passivation layer has formed, showing a steady trend and low current values.

Titanium

The behaviour of titanium was investigated by linear sweep voltammetry starting from the OCP towards 1.75 V and 5.15 V (Fig. 5). The overpotential for hydrogen evolution is greater on titanium with respect to the other investigated metals. In fact, at low electrolyte concentration, the cathodic current onset is below 2 V. Notably, the onset of reduction reactions is the same for all the solutions and is measured as 2.04 ± 0.04 V. On the other hand, the anodic current onset shifts to more positive potentials with the increase of the salt

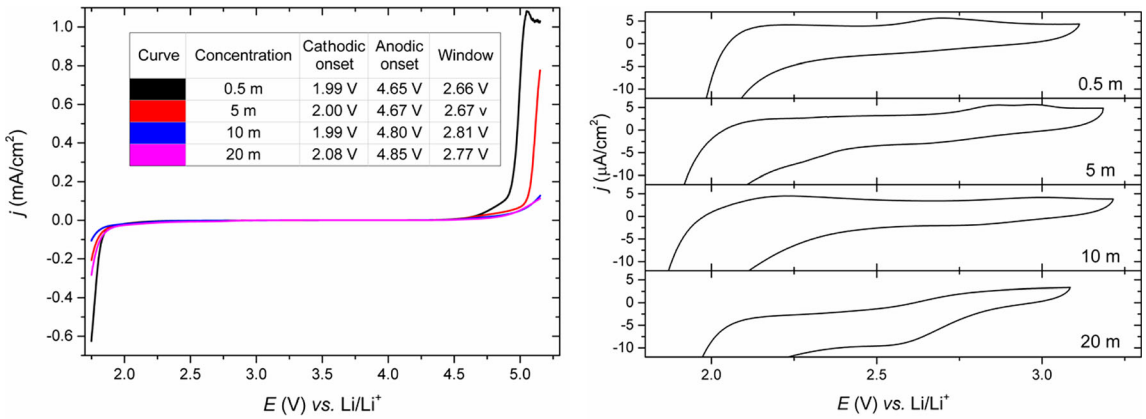

Fig. 5 (a) Linear sweep voltammetries and (b) CVs in the lowest potential range of titanium in aqueous LiTFSI solutions at different salt concentrations

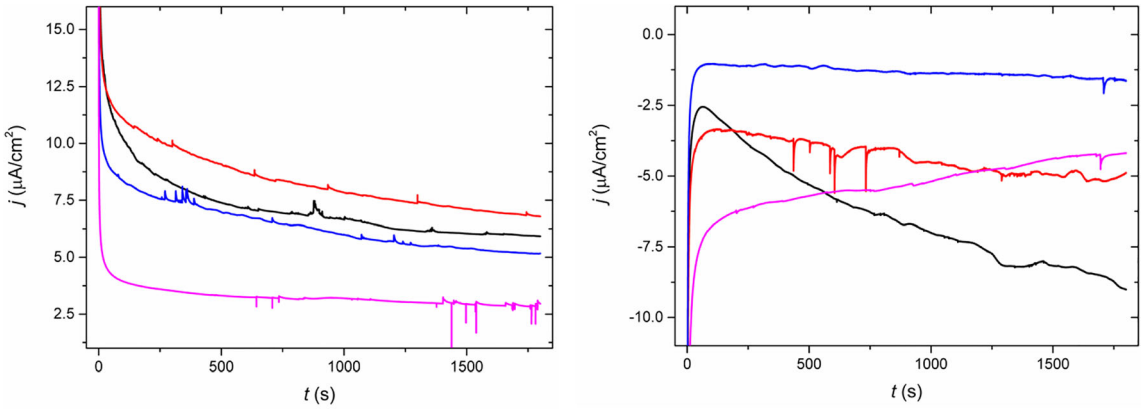

Fig. 6 Chronoamperometric measurements performed at constant potential of (a) 2.15 V (cathodic) and (b) 4.75 V (anodic). Black, 0.5 m; red, 5 m; blue, 10 m; pink, 20 m

concentration (Fig. 5a). Observing the CVs recorded between the OCP and the cathodic limit (Fig. 5b), in the 20 m solution, there is an initial onset at 2.75 V followed by a plateau suggesting the formation of a passivating layer on the metal surface [10].

The cathodic and anodic chronoamperometric measurements were carried out at potentials of 2.15 V and 4.75 V respectively. Under the cathodic stress (Fig. 6a), the decomposition of salt is evident for the 0.5 m and 5 m solution as it is indicated by the increase of current over time. The same trend, although less evident, can also be noticed in the case of the 10 m solution. On the other hand, the 20 m solution, compatibly with what emerged from the CV, initially shows higher currents, but then they decrease as the passivation layer develops. During the anodic stress (Fig. 6b), the current tends to decrease over time regardless salt concentration. A stable condition is achieved with the solutions with higher concentrations, and mainly with the 20 m solution.

Figure 7 compares two consecutive CVs carried out between the OCP and the anodic limit with titanium and steel in 20 m solution. The figure highlights the higher anodic stability of titanium with respect to steel. Furthermore, during the second cycle, the current decreases considerably in the case of titanium, while it remains almost unchanged in the case of the steel collector.

The different anodic behaviour of titanium and steel can be explained by considering their different inherent reactivity towards the formation of surface passivating layers. It is known that with titanium it is possible going to very positive potentials, in some applications even tens of volts are used [24]. This is due to the formation of a compact titanium oxide layer which protects the metal surface. Titania is not an insulator, and in fact it is used as a support in solar and fuel cells; however, the higher the potential applied, the greater the thickness of oxide that is formed, which has a considerably lower conductivity than metals [25], limiting the current flow. It can be argued that titania is formed on the titanium grid even during the anodic scan in LiTFSI aqueous solution so that the 2nd cycle CV currents are lower than those of the first CV.

At the contrary, at positive potentials, steel forms porous and partially soluble iron oxides and hydroxides that do not insulate the metal surface. Hence, steel maintains high conductivity and a good connection with the electrolyte, which explains the overlapping voltammograms of the first and second CV cycle. Furthermore, the oxidation of the steel is, at least in part, reversible. This is suggested by the reduction peak that is present at potentials lower than 3.5 V and that is not present in the case of titanium. Indeed, the formation of titanium oxide is irreversible.

Microscopic characterization

The SEM analysis of the samples performed after the chronoamperometric stress did not report any significative sign of corrosion with respect to the fresh samples that were not subjected to any stress. This observation confirms the

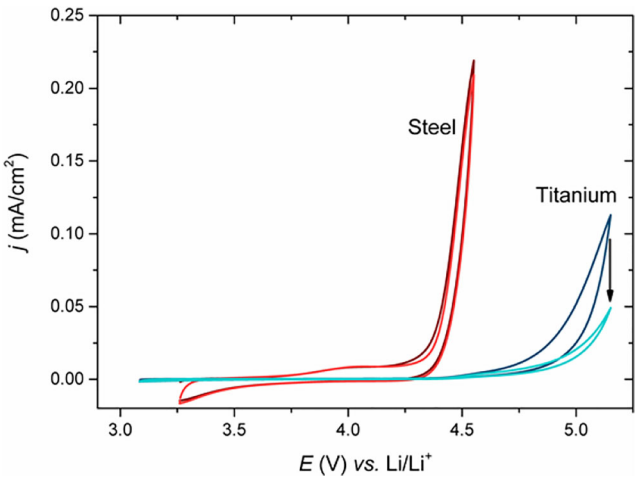

Fig. 7 Consecutive CVs on Ti and steel collector in 20 m aqueous solution of LiTFSI in the high potential range dark red, 1st cycle steel; light red, 2nd steel; dark blue, 1st cycle Ti; light blue, 2nd cycle Ti

formation of a thin passivation layer on the collectors. In Fig. 8, we reported the SEM analysis performed on the untreated collectors meshes (a, steel; d, copper; g, titanium) and the collector after the chronoamperometric, stress, anodic as well as cathodic in the 0.5 m solution. The remaining SEM analysis can be found in the supplementary materials.

Only the copper mesh subjected to anodic potential looks visibly eroded (Fig. 8e). The untreated steel sample (Fig. 8a) presents some dark areas on the surface; the same stains are steel present also in some steel samples after the cathodic stress, while we did not find them in the samples subjected to anodic stress. On the

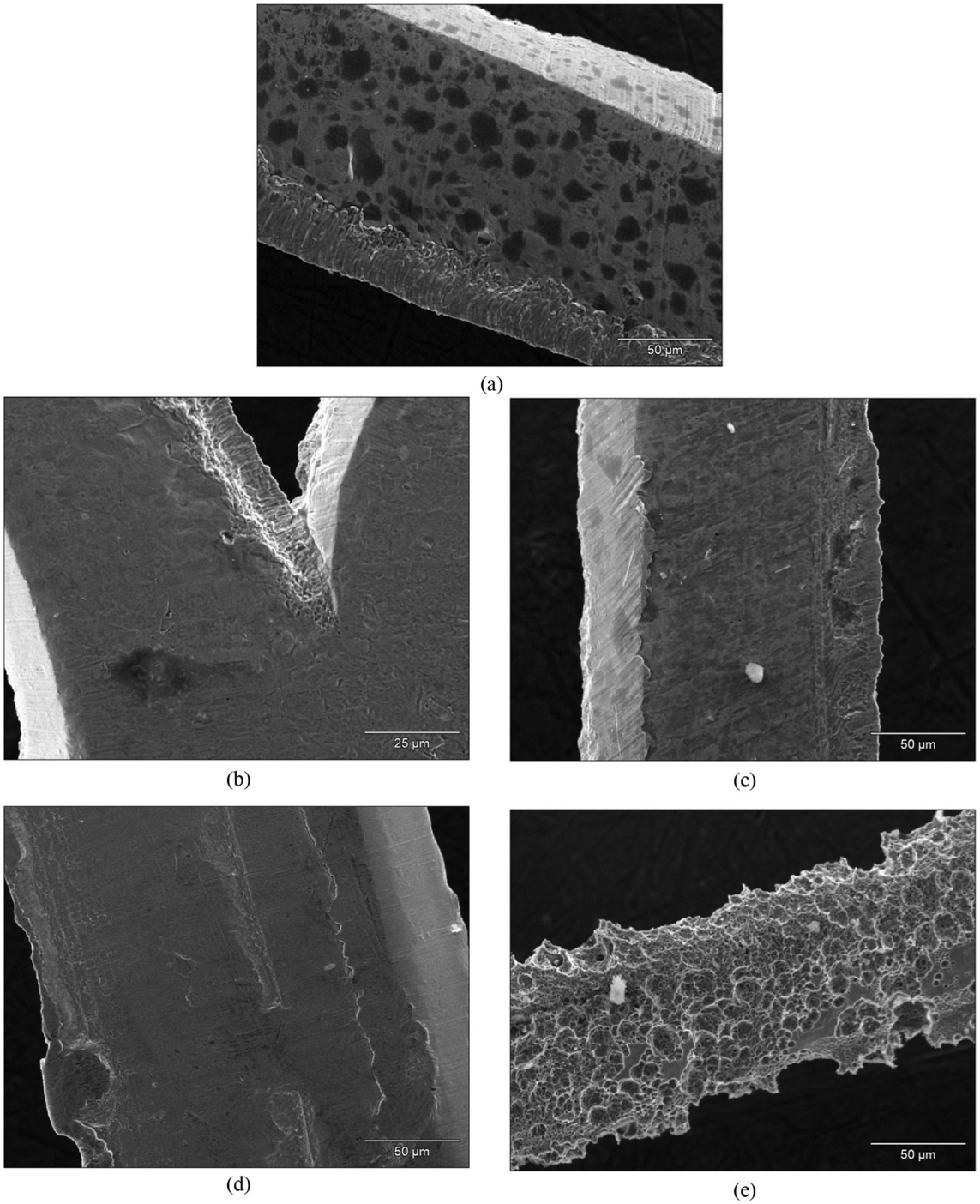

Fig. 8 SEM analysis of the untreated collectors and the cathodic and anodic stressed collectors in 0.5 m solution, the remaining analyses are reported in the supplementary material. (a) Untreated steel; (b) cathodically stressed steel; (c) anodically stressed steel; (d) untreated copper; (e) cathodically stressed copper; (f) anodically stressed copper; (g) untreated titanium; (h) cathodically stressed titanium; (i) anodically stressed titanium

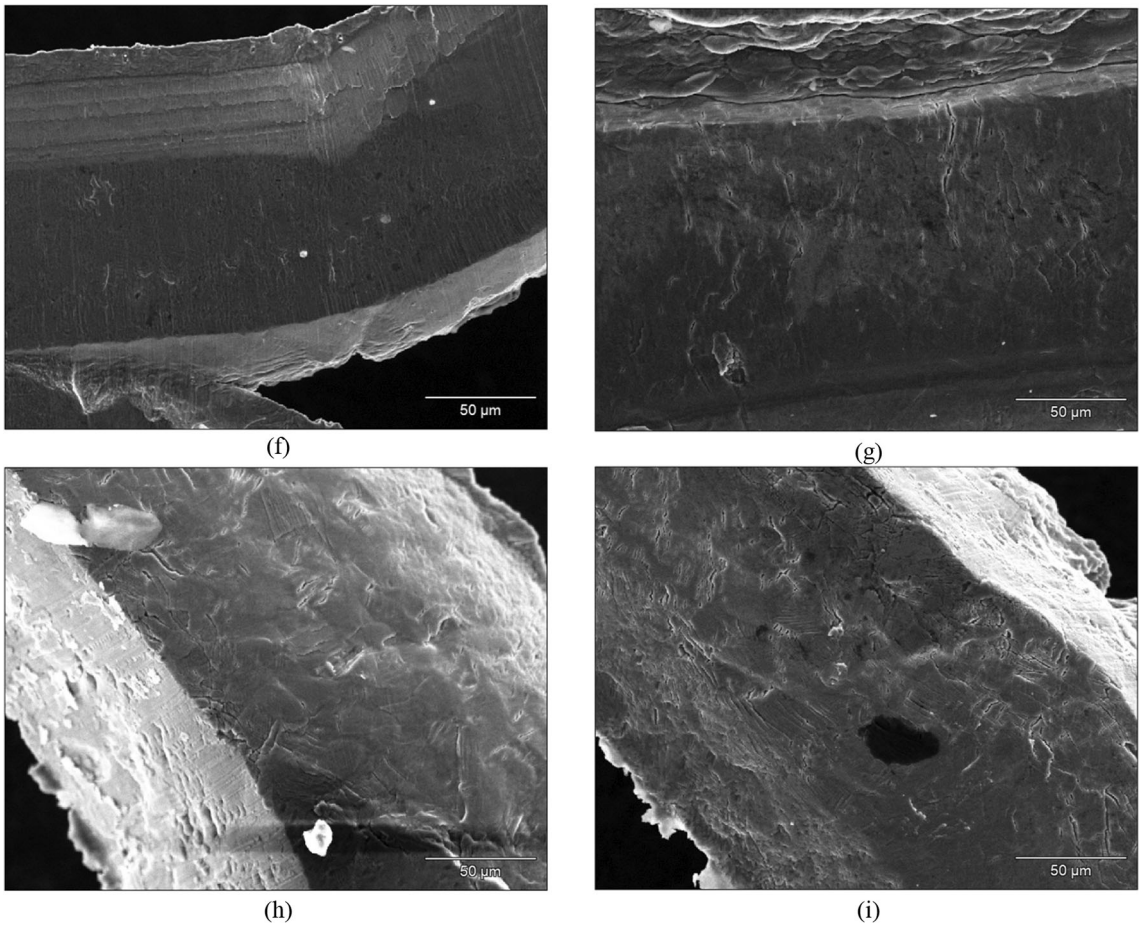

Fig. 8 (continued)

surface of the electrode, we did not find many electrolyte residues.

Spectroscopic characterization

XPS analyses were used to characterize the surface of titanium and steel samples, which exhibited better electrochemical stability with respect to copper. The spectroscopic characterization was performed on fresh meshes of the two materials, used as references, and on the samples tested by anodic and cathodic chronoamperometric ageing in 0.5 m and 20 m solutions, representing the extreme of the investigation.

The analysis of steel samples in the region of Fe (Fig. 9a) showed three components in zone 2p of iron at 706.5 eV, 710 eV, and 712 eV corresponding to metallic iron and iron oxide/hydroxide. Due to the very superficial nature of the technique, the metal iron signal is not very intense. The iron oxide signal is present in all the samples, even in the reference because of the natural passivation layer present on the collector surface. The amount of Fe(II) is substantially unchanged between the reference and the sample subjected to 2.15 eV (cathodic stress) in the 20 m solution; in all other cases, the signal is more intense with respect to the reference. However, by comparing this quantity for the anodic stresses conducted at 4.25 eV, it is observed that the sample analysed in the 20 m solution is less oxidized.

About the steel sample, greater attention was paid to the signals coming from the presence of iron and oxygen, as the former is the element constituting the steel in greater quantities and the oxygen is directly involved in the determination of the degree of collector corrosion.

The presence of oxygen in the surface layer has been confirmed in the transition region 1s (Fig. 9b). In this case, we found the convolutions of 4 signal to the overall peak; the contribution at lower energies around the value of 530 eV is compatible with an iron oxide FeO/Fe_2O_3 structure confirming the trend discussed for the Fe(II) signal.

The measurements carried out on the titanium collectors revealed a similar trend to what was observed on the steel specimens. In the 2p transition region of Ti (Fig. 10), we found two contributions: one at 454 eV, corresponding to metallic titanium, and one at 458 eV, for the Ti(IV) specie. The amount of Ti(IV) is similar between the reference and the sample subjected to cathodic stress in the 20 m solution and increase a little in the case of 0.5 m solution. On the other hand, we found a large amount of titanium oxide in the

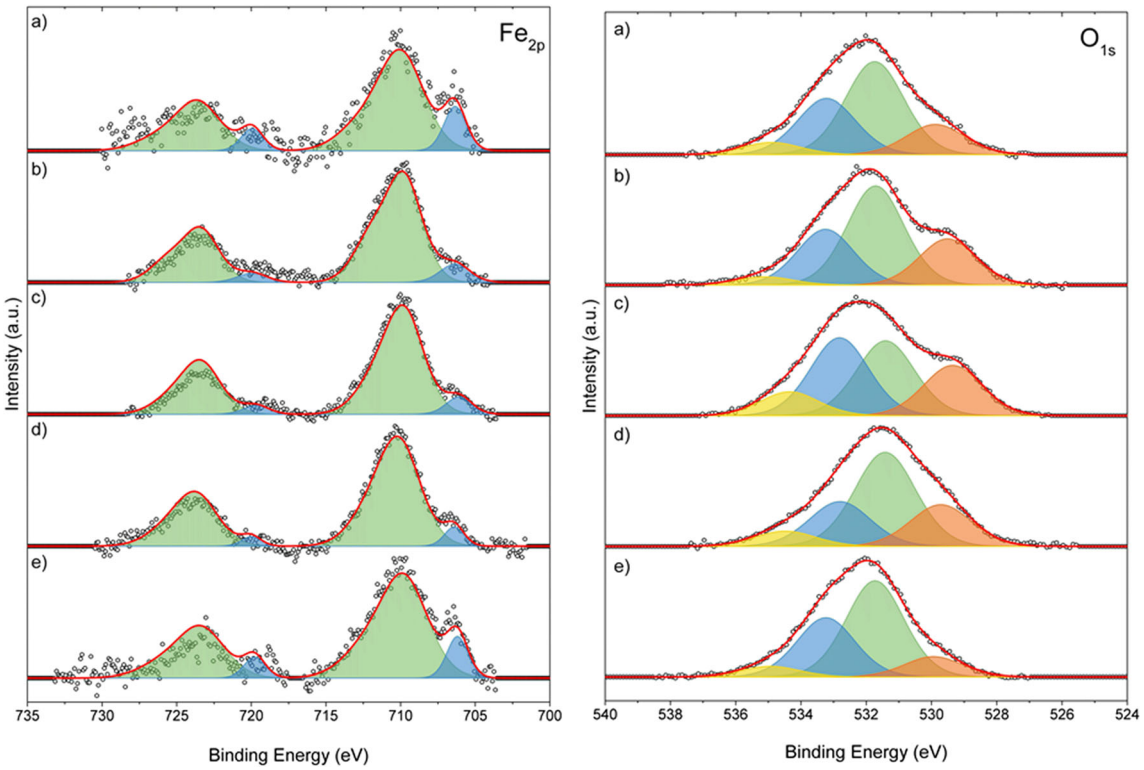

Fig. 9 XPS measurement of steel samples in the Fe 2p region (left) and O 1s region (right): (a) untreated sample; (b) anodically treated sample in 0.5 m solution; (c) anodically treated sample in 20 m solution; (d) cathodically treated sample in 0.5 m solution; (e) cathodically treated sample in 20 m solution

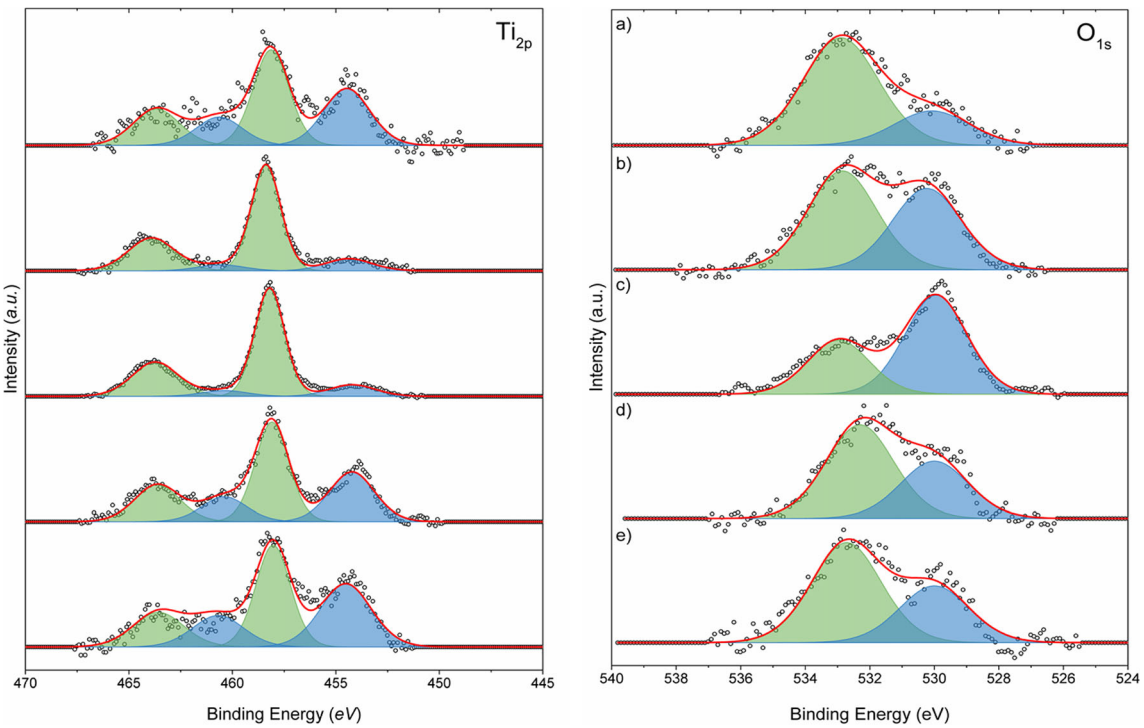

Fig. 10 XPS measurement of titanium samples in the Ti 2p region (left) and O 1s region (right): (a) untreated sample; (b) anodically treated sample in 0.5 m solution; (c) anodically treated sample in 20 m solution; (d) cathodically treated sample in 0.5 m solution; (e) cathodically treated sample in 20 m solution

collectors subjected to anodic stress. Through the tabulated values of the various binding energy related to oxygen, the signal that appears at 530 eV is compatible with the TiO_2 species and follows the same trend of Ti(IV) signal.

Conclusions

In this work, we studied the behaviour of different metal meshes for the application as current collectors in "water-in-salt" cells. In this type of electrolyte, the activity of the water is greatly reduced allowing to extend the electrochemical window. Nonetheless, the copper samples went through a rapid anodic corrosion and did not perform well even in the cathodic potential range. Steel and titanium on the other hand showed an electrochemical window much higher than 1.23 V, and of 2.50 V and 2.80 V respectively. Steel is better in the cathodic onset while titanium features a better anodic stability. Therefore, cells with different current collectors for the positive and negative electrodes could feature an even wider elecotrochemical stability window. In the case of titanium, the anodic window could be further enlarged thanks to the formation of a passivating and semi-conductive layer of titania, that, however, reduces and insulates the electrodes and might increase electrode impedance.

Acknowledgements The authors acknowledge the support that has been given from Freschi & Vangelisti S.r.l. The Italy-South Africa joint Research Programme 2018–2020 (Italian Ministers of Foreign Affairs and of the Environments) is also acknowledged.

Funding This research was funded by the PRIN ("Progetti di Ricerca di Rilevante Interesse Nazionale"), by the project "Novel Multilayered and Micro-Machined Electrode Nano-Architectures for Electrocatalytic Applications (Fuel Cells and Electrolyzers)", grant number 2017YH9MRK and by the Italy-South Africa joint Research Programme 2018–2020. Open access funding provided by Alma Mater Studiorum - Università di Bologna within the CRUI-CARE Agreement.

References

1. Dunn B, Kamath H, Tarascon J-M (2011) Electrical energy storage for the grid: a battery of choices. Science 334:928–935
2. Scrosati B, Garche J (2010) Lithium batteries: status, prospects and future. J Power Sources 195(9):2419–2430
3. Tarascon J-M, Armand M (2001) Issues and challenges facing rechargeable lithium batteries. Nature 414(6861):359–367
4. Goodenough JB, Kim Y (2010) Challenges for rechargeable Li batteries †. Chem Mater 22(3):587–603
5. Lux SF, Terborg L, Hachmöller O, Placke T, Meyer HW, Passerini S, Winter M, Nowak S (2013) LiTFSI stability in water and its possible use in aqueous lithium-ion batteries: pH dependency, electrochemical window and temperature stability. J Electrochem Soc 160(10):A1694–A1700
6. Kim H, Hong J, Park K et al (2014) Aqueous rechargeable Li and Na ion batteries. Chem Rev 114(23):11788–11827
7. Wessells C, Huggins RA, Cui Y (2011) Recent results on aqueous electrolyte cells. J Power Sources 196(5):2884–2888
8. Qu Q, Fu L, Zhan X, Samuelis D, Maier J, Li L, Tian S, Li Z, Wu Y (2011) Porous LiMn2O4 as cathode material with high power and excellent cycling for aqueous rechargeable lithium batteries. Energy Environ Sci 4(10):3985
9. Wang X, Hou Y, Zhu Y, Wu Y, Holze R (2013) An aqueous rechargeable lithium battery using coated Li metal as anode. Sci Rep 3(1):1401
10. Suo L, Borodin O, Gao T et al (2015) "Water-in-salt" electrolyte enables high-voltage aqueous lithium-ion chemistries. Science 350:938–943
11. Bu X, Su L, Dou Q, Lei S, Yan X (2019) A low-cost "water-in-salt" electrolyte for a 2.3 V high-rate carbon-based supercapacitor. J Mater Chem A 7(13):7541–7547
12. Suo L, Borodin O, Wang Y, Rong X, Sun W, Fan X, Xu S, Schroeder MA, Cresce AV, Wang F, Yang C, Hu YS, Xu K, Wang C (2017) "Water-in-Salt" electrolyte makes aqueous sodium-ion battery safe, green, and long-lasting. Adv Energy Mater 7(21):1701189
13. Dong Q, Yao X, Zhao Y, Qi M, Zhang X, Sun H, He Y, Wang D (2018) Cathodically stable Li-O2 battery operations using water-in-salt electrolyte. Chem 4(6):1345–1358
14. Lannelongue P, Bouchal R, Mourad E, Bodin C, Olarte M, le Vot S, Favier F, Fontaine O (2018) "Water-in-Salt" for supercapacitors: a compromise between voltage, power density, energy density and stability. J Electrochem Soc 165(3):A657–A663
15. Suo L, Han F, Fan X, Liu H, Xu K, Wang C (2016) "Water-in-Salt" electrolytes enable green and safe Li-ion batteries for large scale electric energy storage applications. J Mater Chem A 4(17):6639–6644
16. Kühnel R-S, Lübke M, Winter M, Passerini S, Balducci A (2012) Suppression of aluminum current collector corrosion in ionic liquid containing electrolytes. J Power Sources 214:178–184
17. Kühnel R-S, Reber D, Remhof A, Figi R, Bleiner D, Battaglia C (2016) "Water-in-salt" electrolytes enable the use of cost-effective aluminum current collectors for aqueous high-voltage batteries. Chem Commun 52(68):10435–10438
18. Ma T, Xu G-L, Li Y, Wang L, He X, Zheng J, Liu J, Engelhard MH, Zapol P, Curtiss LA, Jorne J, Amine K, Chen Z (2017) Revisiting the corrosion of the aluminum current collector in lithium-ion batteries. J Phys Chem Lett 8(5):1072–1077
19. Theivaprakasam S, Girard G, Howlett P et al (2018) Passivation behaviour of aluminium current collector in ionic liquid alkyl carbonate (hybrid) electrolytes. npj Mater Degrad 2:13
20. Parsons R (1967) Atlas of electrochemical equilibria in aqueous solutions. J Electroanal Chem Interfacial Electrochem 13:471
21. Zhang X, Devine TM (2006) Passivation of aluminum in lithium-ion battery electrolytes with LiBOB. J Electrochem Soc 153(9):B365
22. Shirley DA (1972) High-resolution X-ray photoemission spectrum of the valence bands of gold. Phys Rev B 5(12):4709–4714

23. Susi T, Pichler T, Ayala P (2015) X-ray photoelectron spectroscopy of graphitic carbon nanomaterials doped with heteroatoms. Beilstein J Nanotechnol 6:177–192
24. Karambakhsh A, Afshar A, Ghahramani S, Malekinejad P (2011) Pure commercial titanium color anodizing and corrosion resistance. J Mater Eng Perform 20(9):1690–1696
25. Alivov Y, Fan ZY, Johnstone D (2009) Titanium nanotubes grown by titanium anodization. J Appl Phys 106(3):034314